Understanding Confinement in Advanced Inductive Scenario Plasmas — Dependence on Gyroradius and Rotation

P.A. Politzer[1], C.D. Challis[2], E. Joffrin[3], T.C. Luce[1], M. Beurskens[2], P. Buratti[4], F. Crisanti[4], J.C. DeBoo[1], J.R. Ferron[1], C. Giroud[2], J. Hobirk[5], C.T. Holcomb[6], A.W. Hyatt[1], F. Imbeaux[3], R.J. Jayakumar[1], I. Jenkins[2], J.E. Kinsey[1], R.J. La Haye[1], D.C. McDonald[2], C.C. Petty[1], F. Turco[7], M.R. Wade[1], and JET EFDA Contributors*

[1]General Atomics, PO Box 85608, San Diego, California 92186-5608, USA
[2]EURATOM/CCFE Fusion Association, Culham Science Centre, Abingdon, Oxon OX14 3DB, UK
[3]Associatione Euratom CEA, CEA/DSM/IRFM, Cadarache, 13108 Saint-Paul-lez-Durance, France; JET-EFDA-CSU Culham Science Center, Abingdon, OX14 3DB, UK
[4]Associazione Euratom-ENEA sulla Fusione, CR Frascati, Via E Fermi 45 00044 Frascati (Roma), Italy
[5]Max-Planck-Institut für Plasmaphysik, Euratom Association, 85748, Garching, Germany.
[6]Lawrence Livermore National Laboratory, Livermore, California 94550, USA
[7]Oak Ridge Institute for Science Education, Oak Ridge, Tennessee 37830-8050, USA

e-mail: politzer@fusion.gat.com

Abstract. Advanced inductive (AI) plasmas are a realization of the ITER hybrid scenario, providing high neutron fluence in a long inductive discharge. The physics of AI plasmas has not been investigated as thoroughly as for standard ELMy H-mode discharges. In this paper we report new results on the dependence of confinement in AI plasmas on several key parameters. A joint JET and DIII-D experiment has studied the scaling of confinement with normalized plasma size or ion gyroradius ($\rho_* = \rho_i/a$). This study spans a range in ρ_* of 2.7, roughly equal to the range from JET to ITER. The significant preliminary results are: (i) a good identity match has been demonstrated, confirming the validity of the study, (ii) the global scaling of the energy confinement time is roughly Bohm-like, $B\tau_E \propto \rho_*^{-1.91}$, and (iii) the local thermal diffusivities (assuming $\chi/\chi_B \propto \rho_*^{\alpha}$) scale as α_e = -0.24 to -0.74 and α_i = -0.42 to -0.69, depending on location within the plasma. We also report on the dependence of confinement in AI plasmas in DIII-D on rotation and on the presence of a neoclassical tearing mode (NTM). We find that the overall increase in energy confinement time from the minimum to the maximum accessible rotation is as much as 40%. Over the same rotation range, the estimated reduction in τ_E due to the NTM decreases by up to 6%. We estimate that, at the highest rotation, the NTM has a 5%–10% effect on τ_E. Also, extending the analysis of DIII-D experiments using electron cyclotron heating (ECH) to study the influence of varying T_e/T_i on confinement shows that the density reduction often seen with ECH is directly coupled to the change in rotation and is only indirectly due to changing T_e/T_i via modification of momentum transport.

1. Gyroradius Scaling

Advanced inductive (AI) scenario plasmas have the potential for long pulse tokamak operation and high fusion yield. Extrapolation of the performance of these scenarios depends on the scaling of transport with machine size, which may not be correctly described by the present empirical scaling rules for standard edge localized mode (ELM)y H-mode plasmas, e.g., the ITER98(y,2) scaling [1]. Determination of the dependence of plasma performance on dimensionless physical parameters is a robust and rigorous method for development of scaling laws and for the prediction of the characteristics of plasmas in future confinement facilities such as ITER [2]. In particular, determining the scaling with is ρ_* is important because the variation in other important dimensionless parameters between present tokamaks and ITER can be made small, whereas the ρ_* value in ITER is presently inaccessible at high performance.

To develop the dimensionless scaling of AI plasmas, JET and DIII-D have carried out a ρ_* scan across both machines, spanning a range of 2.7, much larger than can be done in any

*See the Appendix of F. Romanelli et al., paper OV/1-3, this conference.

single tokamak. Also, this is approximately equal to the range from JET to ITER, adding additional confidence to the extrapolation. To establish the validity of the dimensionless scaling approach, an identity comparison between the two tokamaks was also done.

Although different techniques are used to establish AI discharges in the two devices, the performance characteristics are similar, indicating the robustness of the scenario (Fig. 1). Typically, DIII-D uses heating early in the current ramp in order to prevent current penetration and form a broad q profile. An NTM (usually $m/n = 3/2$) appears early in the high β phase and has been shown to help maintain a broad, stationary q profile [3]. In JET, good performance AI plasmas are established by using an overshoot in the current to produce the desired q profile [4]. While this profile slowly relaxes, there are several seconds of high performance AI operation.

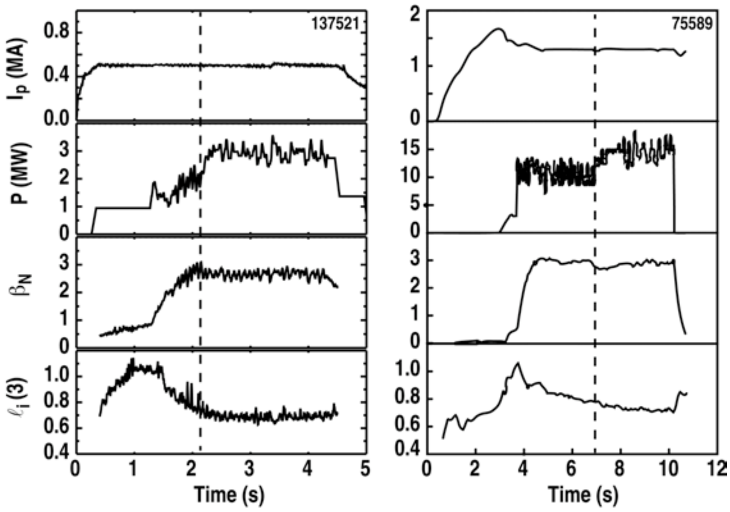

FIG. 1. Time histories of a high ρ_* DIII-D discharge (137521, left) and a low ρ_* JET discharge (75589, right). Note current overshoot used by JET to establish the broad current profile. The onset times of m/n=3/2 NTMs are indicated by the dashed lines. In DIII-D the mode appears at the start of the high β_N time. In JET the mode appears after several seconds at high β_N due to slow evolution of the current profile.

2.1 Matched Discharges

Plasmas with the same shape and aspect ratio were produced in both tokamaks (Fig. 2). Linear dimensions of the plasma in JET were larger by a factor of ~1.67 compared to DIII-D. The shape parameters were constrained by matching the two tokamaks over a range in ρ_*. They differed somewhat from the expected ITER parameters: $\varepsilon = 0.31$ (ITER≈0.32), $\kappa_x = 1.75$ (ITER≈1.85), and $\delta = 0.36$ (ITER≈0.48). The safety factor parameters were $q_{95} = 4.1\text{-}4.6$ and $q_{\min} \approx 1$, with a broad region of low magnetic shear in the plasma core.

In both tokamaks, the heating was done with co-injected energetic neutral beams. The neutral beam (NB) heating power was modulated to maintain constant β. The dimensionless parameters ν_*, β, and M were matched to within 20% at the half-radius.

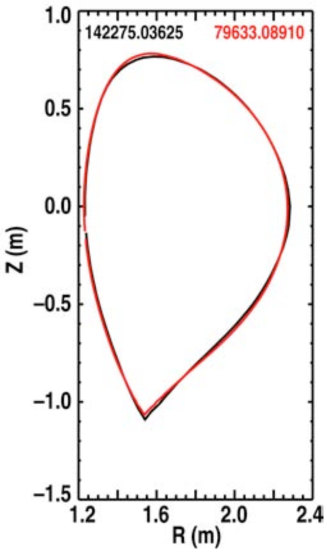

FIG. 2. Overlay of the separatrix shapes of DIII-D discharge 142275 at 3.625 s (black) and JET discharge 79633 at 8.91 s (red). The dimensions of the JET discharge are reduced by a factor of 1.675.

2.2 Global Scaling of Confinement

If a power law dependence of thermal diffusivity on ρ_* ($\chi/\chi_B \propto \rho_*^{\alpha}$; where $\chi_B = T/eB$) is assumed, the thermal energy confinement time should scale like

$B\tau_E = \rho_*^{-(2+\alpha)} F(\nu_*, \beta, q, T_i/T_e, \varepsilon, ...)$, where the arguments of F are the other dimensionless parameters governing confinement. By holding all dimensionless parameters except ρ_* fixed, the dependence of $B\tau_E$ on ρ_* can be determined.

Well-matched time slices from each of four discharges from each tokamak (eight slices in all) were selected for comparison from a database of 19 JET and 12 DIII-D discharges. These show good matches in the n_e, T_e, and T_i profiles, as well as in the derived profiles: β, ν_*, and M. Neoclassical tearing modes (NTMs) were present at very low amplitude or not at all. There are some residual variations of characteristic parameters with ρ_*. In particular, the Mach number is typically somewhat higher in JET than in DIII-D. The current profiles also vary, as indicated by the values of $\ell_i(3)$. Parameters characterizing these two selected sets are compared in Table I.

TABLE 1: Comparison of JET and DIII-D ρ_* Scaling Discharges. The parameters $q_{cyl}^\dagger = 5Ba^2\kappa/IR$, $\nu_{*e}^\dagger = n_e a/T_e^2$, and $\beta_T^\dagger = n_e(T_e+T_i)/B^2$ are evaluated at $\hat{\rho} = 0.5$. Δ is the difference between the JET and DIII-D mean values, and Σ is the sum.

Parameter	JET Mean	DIII-D Mean	Δ/Σ (%)
a/R	0.315	0.298	2.7
κ_a	1.51	1.54	0.7
$q_{cyl}^\dagger$	2.92	2.68	4.4
$\ell_i(3)$	0.854	0.715	8.9
$\nu_{*e}^\dagger$	0.594	0.563	2.7
$\beta_T^\dagger$	5.58	5.45	1.2
T_i/T_e	1.097	1.222	5.4
H_{98y2}	1.29	1.32	1.2

The best fit to these eight plasmas yields $B\tau_E \propto \rho_*^{-1.91}$. As there are small variations in other dimensionless parameters, these can be compensated by assuming a dependence for $B\tau_E$. For example, ITER98(y,2) scaling is $B\tau_E \propto q_{cyl}^{-3}\beta^{0.9}$. With this adjustment, the ρ_* scaling becomes $B\tau_E/q_{cyl}^{-3}\beta^{-0.9} \propto \rho_*^{-2.30}$. If a weaker scaling is used, $q_{cyl}^{-2}\beta^0$, the exponent of ρ_* becomes -2.13.

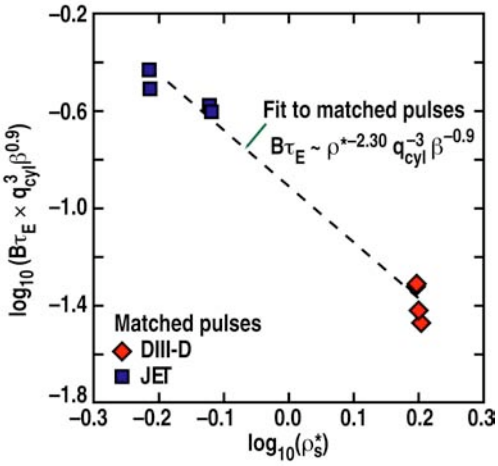

FIG. 3. Normalized energy confinement time plotted vs. ρ_* to determine the global scaling. Here $\rho_s^* = a^{-5/6} B^{-2/3}$.

The ITPA database of hybrid plasmas shows a strong dependence of H_{98y2} on ρ_* [5]. This database contains parameters for a wide variety of discharges from ASDEX Upgrade, DIII-D, and JET. The results presented here show that the apparent variation of H_{98y2} is an artifact of the wide variation in plasma conditions included in the database. Figure 4 shows that, for well-matched plasmas, H_{98y2} is essentially independent of ρ_* over a wide range.

This result does not differentiate among the effects of diffusive transport, pedestal confinement, profile peaking, low-level MHD activity, or differences in Z_{eff} or rotation. To isolate the scaling of diffusive heat transport, it is necessary to look at the dimensionless scaling of the local transport.

2.3 Local Scaling of Transport

The scaling of local transport with the dimensionless parameters can only be obtained by comparing discharges with matched profiles of the observable quantities, particularly n_e, T_e, and T_i. Two separate comparisons of JET and DIII-D results have been undertaken: an identity discharge comparison and a comparison of discharges at the extremes of the accessible range in ρ_* (the highest DIII-D values and the lowest JET values). Good profile matches were found among three JET and eight DIII-D discharges for the identity comparison and eight JET and nine DIII-D discharges for the extended ρ_* comparison. Profiles were compared over the range in normalized radius $0.45 \le \hat{\rho} \le 0.85$, encompassing 52% of the plasma volume. These limits exclude the edge pedestal region where the scaling might differ from that of the bulk and where high spatial resolution profile data is required, as well as the central core region where NTMs and $m/n = 1/1$ MHD activity can occur.

For both comparisons the method used was to determine the best set of matching profiles for each discharge pair (one JET and one DIII-D), and then to sort the discharge pairs according to the goodness-of-fit. The profiles are scaled as appropriate for identity or ρ_* scaling comparison, and a fit parameter is obtained for each quantity (the rms deviation from the mean relative to the mean value). These are combined for each discharge pair to give an overall goodness-of-fit parameter, with n_e, T_e, T_i, and I/aB having equal weight, and Ω_ϕ with half the weight of the others.

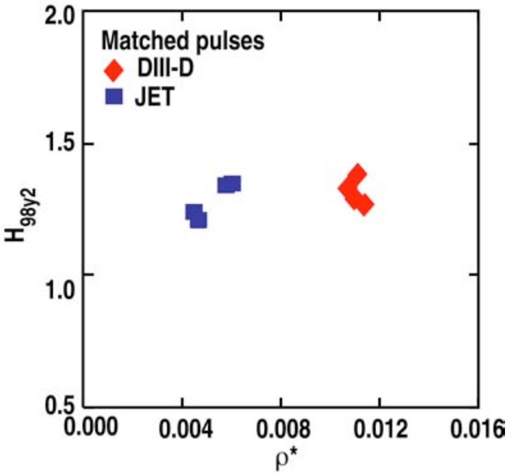

FIG. 4. For well-matched plasmas, H_{98y2} depends very weakly on ρ_*. Values of H_{98y2} in the ITPA database [5] range from 0.5 to 2.0.

The identity comparison entails matching all dimensionless parameters (including ρ_*) and varying only the dimensional parameters. Obtaining a good identity match indicates that the same physics is occurring in both tokamaks, that the important physical phenomena are indeed governed by the same equations and that the set of dimensionless parameters correctly represents these processes. Figure 5 illustrates the matching of the measured profiles for a single pair of discharges. The JET profiles are the direct measurements from the Thomson scattering and charge exchange diagnostics. The DIII-D data have been smoothed with a spline fit. The only significant variation between the scaled profiles is that the scaled JET density is somewhat higher than for DIII-D and has a shorter gradient scale length. Nevertheless the fit parameter for n_e (the rms fractional difference) is 3.5%. The profiles of the computed dimensionless parameters for this case are compared in Fig. 6. The difference in density profiles leads to a small mismatch in β, and the small deviations in the T_e and Ω_ϕ profiles conspire to give a small mismatch in M.

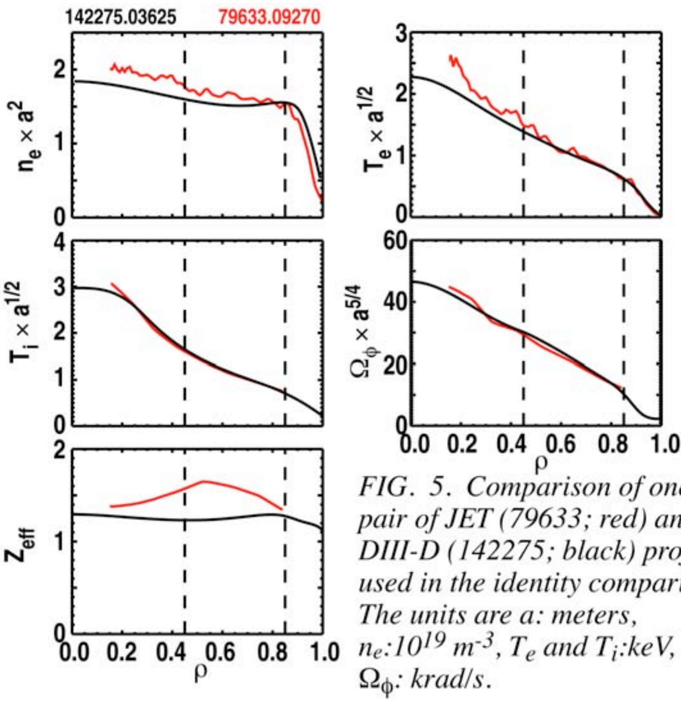

FIG. 5. Comparison of one pair of JET (79633; red) and DIII-D (142275; black) profiles used in the identity comparison. The units are a: meters, n_e: 10^{19} m^{-3}, T_e and T_i: keV, Ω_ϕ: krad/s.

The test of whether the identity match confirms the physics is a comparison of the scaled thermal conductivities. The power balance terms and transport coefficients are determined using TRANSP [6]. We use the conducted heat flux, $q = -n\chi\nabla T$, rather than χ as the measure of diffusive transport because of the noise on the input profiles. Figure 7 plots the scaled profiles of q_e and q_i. The q_e match is good (3.3%) and the q_i match is fair (10.1%). Considering that the identity scaling of the heat flux is $(a_{\text{DIII-D}}/a_{\text{JET}})^{11/4} = 4.1$ this level of agreement between the scaled values of q is sufficient to establish that we are looking at the same physics in both tokamaks. For the ensemble of the 20 best pairs of discharges with respect to an identity match, the mean fit for q_e is 6.1±3.4% and for q_i it is 8.9±4.6%.

The initial assessment of the scaling of thermal transport with ρ_* has been done by comparing the most extreme cases – the lowest JET values and the highest DIII-D values. We selected the 20 best pairs of matched discharges with $\rho_{*\text{DIII-D}}/\rho_{*\text{JET}}\ (\hat{\rho}=0.65) \geq 2.3$. The scaled kinetic profiles for one of these discharge pairs are shown in Fig. 8. The most notable deviations in the profile matches are in the density gradient scale length – again the JET profile is a bit steeper, and in Z_{eff}. The profiles of ν_*, β, and M match very well over the region of interest (Fig. 9), as do the scaled ρ_* profiles.

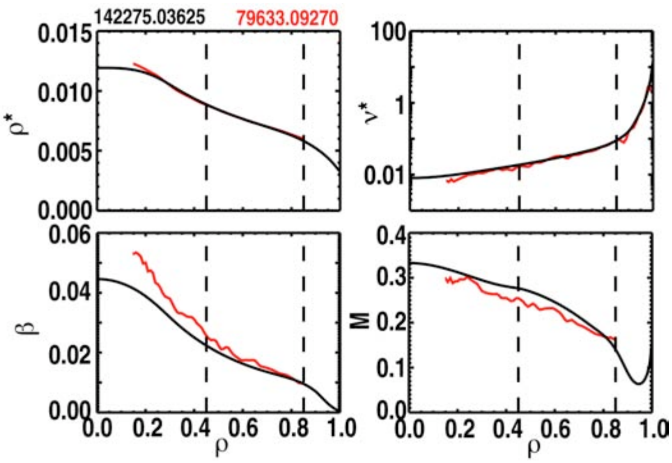

FIG. 6. Profiles of dimensionless parameters for discharges 79633 (red) and 142275 (black).

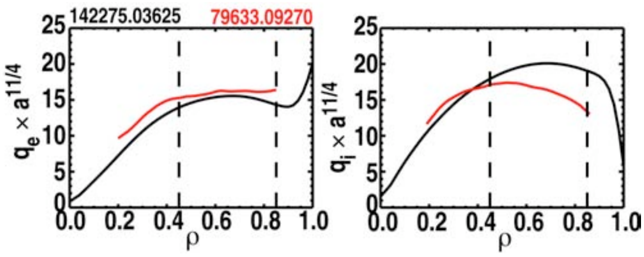

FIG. 7. Scaled heat flux profiles for JET (79633; red) and DIII-D (142275; black). The heat flux is measured in kW/m^2.

We again use the scaled heat flux profiles to determine the exponent α (assuming $\chi/\chi_B \propto \rho_*^\alpha$). For ρ_* scaling, the heat flux should scale as $q \propto a^{-2/3}B^{5/3}$, and the exponent is obtained from $\alpha = \ln(q_1 a_1^{2/3} B_1^{-5/3} /\ q_2 a_2^{2/3} B_2^{-5/3}) / \ln(\rho_{*1}/\rho_{*2})$ where the subscripts 1 and 2 refer to the two matched conditions. The scaled heat fluxes and the derived values of α_e and α_i are plotted in Fig. 10. In this example the value of α_e ranges from -0.01 to -0.55 across the region of interest, and for the ions α_i varies from -0.34 to -0.51. For the ensemble of matched pairs, there is considerable scatter in the values of α, and furthermore, there appears to be a significant dependence on radius across the matching zone. The ensemble averages of α_e at selected locations are -0.24±0.36, -0.42±0.33, and -0.74±0.31 at $\hat{\rho}$ = 0.45, 0.65, and 0.85, respectively. At the same locations, α_i =-0.42±0.25, -0.57±0.27, and -0.69±0.33. These results should be viewed as preliminary. Among the planned improvements in analysis are using motional Stark effect (MSE)-based equilibrium reconstructions to determine q profiles and to map the diagnostic data to flux coordinates; doing suitable spatial and temporal

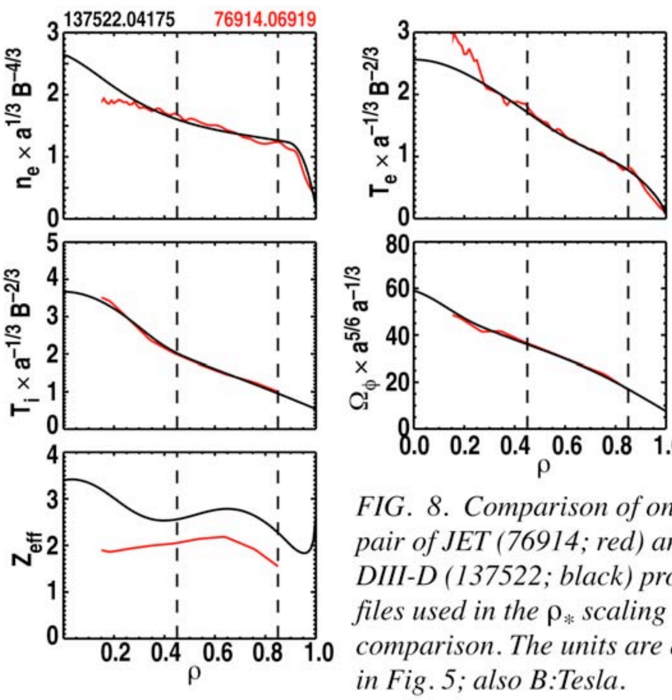

FIG. 8. Comparison of one pair of JET (76914; red) and DIII-D (137522; black) profiles used in the ρ_* scaling comparison. The units are as in Fig. 5; also B:Tesla.

averaging of noisy profile data; and undertaking a more precise power balance analysis including a better estimate of the neutral beam injection (NBI) deposition profile. Nevertheless, the basic trends can be expected to persist, particularly $\alpha_e \geq \alpha_i$ and the decrease of both α_e and α_i with increasing minor radius.

3. Dependence on Rotation

Present experiments differ from ITER and future tokamaks in the magnitude of the expected plasma rotation. Until recently, the experience base for AI discharges has been dominated by plasmas with strong toroidal rotation, using significant levels of NBI co-injection for plasma heating. In recent DIII-D experiments we have studied the changes in characteristics and performance of AI plasmas as the input torque and the resulting toroidal rotation are varied in discharges with similar density and β but a range of q_{95} (3.1–4.9) [7]. The experiments used combinations of co- and counter-NBI with feedback control of β_N. Increasing the rotation by a factor of 3 led to a decrease in the electron and ion thermal diffusivities by a factor of 2, with very little change in the density, temperature, or current profiles (Fig. 11). The momentum diffusivity also increased in the core of the plasma.

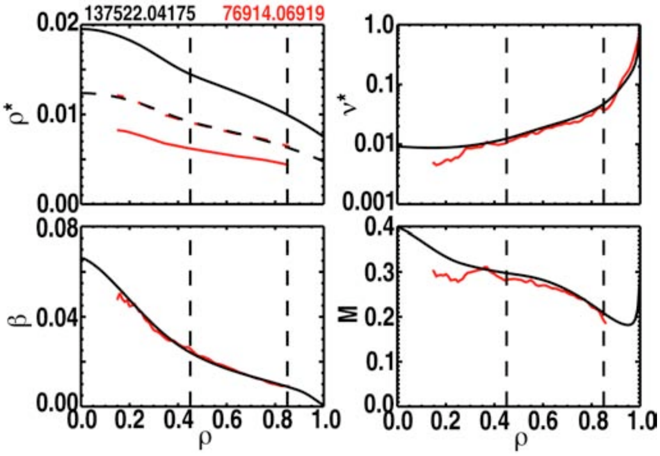

FIG. 9. Dimensionless parameter profiles for discharges 76914 (red) and 137522 (black). β, ν_*, and M match well within the comparison region between the dashed lines. The ρ_* profiles differ by a factor of 5.33. When multiplied by $a^{5/6}B^{2/3}$ (dashed lines) the ρ_* profiles agree.

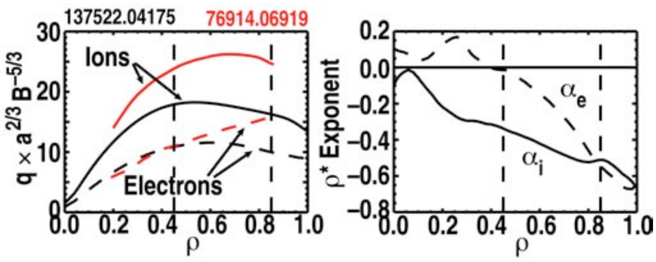

FIG. 10. Heat flux profiles (scaled) for discharges 76914 (red) and 137522 (black). Ion values are shown by solid lines and electron values by dashed lines. Also plotted are the derived exponents of ρ_* in $\chi_{i,e}/\chi_B \propto \rho_*^{\alpha_{i,e}}$.

The lower limit to achievable rotation was set by the penetration of error fields and subsequent locking. From the lowest accessible rotation to the highest, a range of ~4.6, H_{89} [8] increased from ~2.0 to ~2.5 and H_{98y2} from ~1.1 to ~1.4, with a weak dependence on q_{95} (Fig. 12). Modeling using the GLF23 code indicates that the dominant effect is the increase in $E \times B$ flow shear, with an accompanying decrease in low- and intermediate-k turbulence. At low rotation an equally good fit is obtained with and without the flow shear terms.

The energy confinement time in the lower q_{95} plasmas were more sensitive to changes in rotation, largely because the $m/n = 3/2$ NTM island width increases as q_{95} is reduced and because the $q = 2$ surface is at larger $\hat{\rho}$, allowing the islands to affect a larger fraction of the plasma volume. Figure 13 shows the change in island width with rotation estimated on the basis of magnetic probe signals and the radial location. The location of the $q = 2$ surface is $\hat{\rho} \approx 0.44$ for $q_{95} = 4.5\text{-}4.9$ and $\hat{\rho} \approx 0.59$ for $q_{95} = 3.1\text{-}3.4$. (Note that for fixed q_{95} the q profile does not change when the rotation changes.) Figure 13 also shows the estimated change in energy confinement time due to the presence of the NTM. The strongest effect is for low q_{95} at low rotation, where ~15% of the energy confinement is lost, compared to a hypothetical case with no NTM. However, the difference between the maximum and

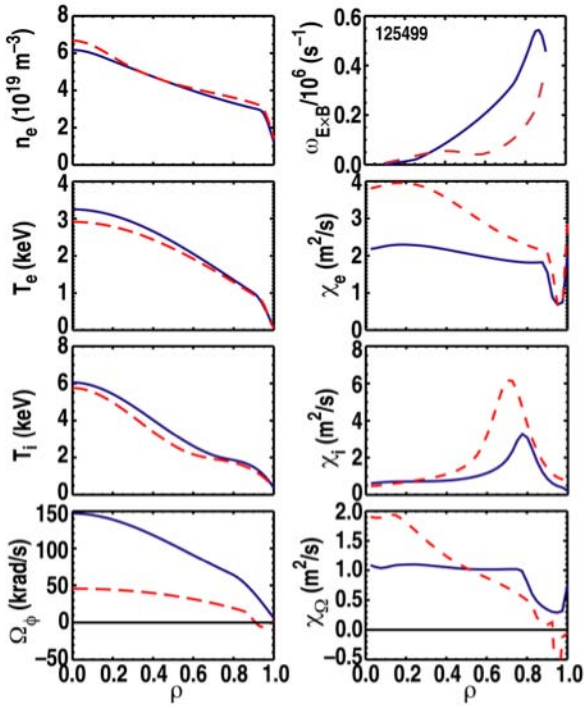

FIG. 11. Profiles for DIII-D discharge 125499 at times of high rotation (solid, blue) and low rotation (dashed, red).

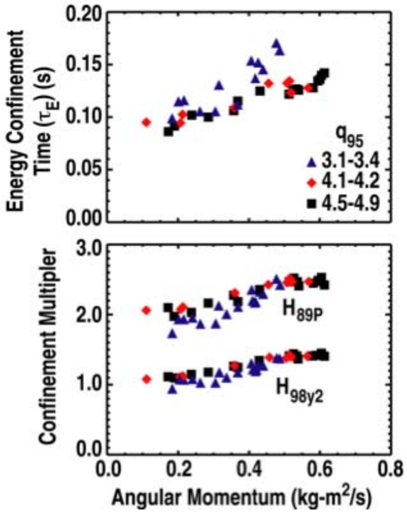

FIG. 12. Energy confinement time and confinement scaling multipliers (H_{89P} and H_{98y2}) as a function of toroidal angular momentum for three ranges of q_{95} as indicated in the legend.

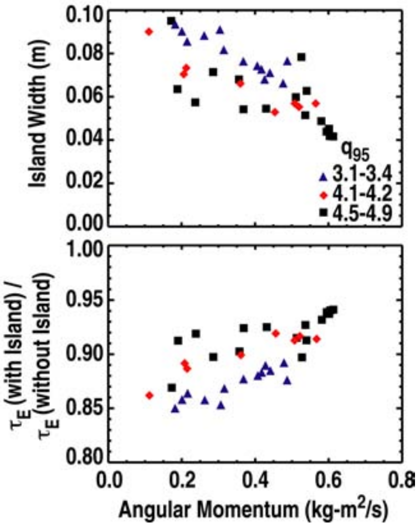

FIG. 13. Variation of the $m/n = 3/2$ NTM island width and the estimated energy confinement time penalty due to the NTM as a function of toroidal angular momentum, for the same data set shown in Fig. 12.

minimum rotation cases is only 4%-6% for all values of q_{95}. Comparing Figs 12 and 13 we see that the effect of decreasing 3/2 island width, while less important than the changing $E \times B$ flow shear, is not negligible.

4. An Observation on T_e/T_i Effects

Experiments at DIII-D have also addressed the dependence of confinement on T_e/T_i [9]. Adding electron cyclotron heating (ECH) to an AI scenario plasma increased T_e/T_i but also increased energy and momentum transport. Further analysis of these studies shows that, in addition to the effect on momentum and energy confinement, particle transport is strongly coupled to rotation. Figure 14 compares two AI discharges, matched in β and central rotation. One has only co-injected NBI plus ECH, and the other has no ECH but uses co- plus counter-NBI to produce the same β and rotation. Note that the reduction in density is the same when either the ECH or counter-NBI is added, even though T_e/T_i is different. This appears to indicate that the increase in particle transport is coupled to the decrease in rotation rather than to the direct effect of ECH on T_e/T_i. The effect is thus presumably indirect, via the effect of changing T_e/T_i on momentum transport.

5. Summary & Conclusions

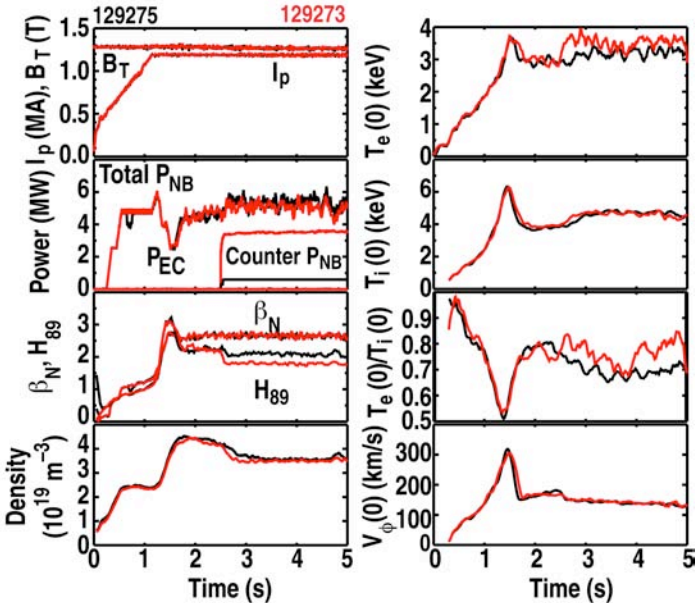

FIG. 14. Comparison of two discharges, matched in β and rotation. One (129273; red) uses electron cyclotron frequency heating with all co-NBI. The other (129275; black) uses no ECH, but reduces the rotation with added counter-NBI.

AI plasmas are a realization of the ITER hybrid scenario, providing high neutron fluence in a long inductive discharge. We report here new results on the dependence of confinement in AI plasmas on several key parameters. A joint JET and DIII-D experiment has studied the scaling of confinement with normalized plasma size or ion gyro-radius (ρ_*). This study spans a range in ρ_* of 2.7, roughly equal to the range from JET to ITER. The significant preliminary results are: (i) a good identity match has been demonstrated, confirming the validity of the study, (ii) the global scaling of the energy confinement time is roughly Bohm-like, $B\tau_E \propto \rho_*^{-1.91}$, and (iii) the local thermal diffusivities (assuming $\chi/\chi_B \propto \rho_*^{\alpha}$) scale as α_e = -0.24 to -0.74 and α_i = -0.42 to -0.69, depending on location within the plasma (from $\hat{\rho}$ = 0.45 to 0.85). This scaling with ρ_* is similar to that found for L-mode, and is less favorable than the conventional H-mode scalings (ITER98(y,2), DS03). However projection to ITER must also take into account the dependences on collisionality, rotation, and T_e/T_i. Until these are determined, a definitive projection to ITER cannot be done.

We also present new results on the dependence of confinement in AI plasmas in DIII-D on rotation and on the presence of an NTM. We find that the overall increase in energy confinement time from the minimum to the maximum accessible rotation is as much as 40%. Over the same rotation range, the estimated reduction in τ_E due to the NTM decreases by up to 6%. We estimate that, at the highest rotation, the NTM has a 5%-10% effect on τ_E. Also, extending the analysis of DIII-D experiments using ECH to study the influence of varying T_e/T_i on confinement shows that the density reduction often seen with ECH is directly coupled to the change in rotation and is only indirectly due to changing T_e/T_i via modification of momentum transport.

This work was supported in part by the US Department of Energy under DE-FC02-04ER54698, DE-AC52-07NA27344, and DE-AC05-06OR23100 and by EURATOM within the framework of the European Fusion Development Agreement.

References

[1] ITER Physics Basis 1999, Nucl. Fusion **39** (1999) 2204
[2] LUCE, T.C., et al., Plasma Phys. Control. Fusion **50** (2008) 043001
[3] POLITZER, P.A., et al., Proc. of 32nd EPS Conf. on Plasma Physics, vol 29C (ECA, 2005) 0-1.001
[4] JOFFRIN, E., et al., Proc. of 22nd IAEA Fusion Energy Conf., Geneva, 2008, IAEA-CN-165/EX/1-4Ra
[5] McDONALD, D.C., et al., Plasma Phys. Control. Fusion **50** (2008) 12401
[6] GOLDSTON, R.J., et al., J. Comput. Phys. **43** (1981) 61
[7] POLITZER, P.A., et al., Nucl. Fusion **48** (2008) 075001
[8] YUSHMANOV, P.N., et al., Nucl. Fusion **30** (1990) 1999
[9] PETTY, C.C., et al., Proc. of 22nd IAEA Fusion Energy Conf., Geneva, 2008, IAEA-CN-165/EX/1-4Rb